Heating Characteristics of Convection Reflow Ovens

Balázs Illés, Gábor Harsányi

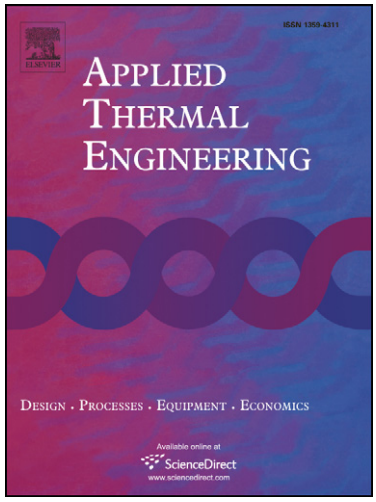

Heating Characteristics of Convection Reflow Ovens

Balázs Illés, Gábor Harsányi

PII: S1359-4311(08)00437-7
DOI: 10.1016/j.applthermaleng.2008.10.014
Reference: ATE 2650

To appear in: *Applied Thermal Engineering*

Received Date: 2 April 2008
Revised Date: 10 October 2008
Accepted Date: 30 October 2008

Please cite this article as: B. Illés, G. Harsányi, Heating Characteristics of Convection Reflow Ovens, *Applied Thermal Engineering* (2008), doi: 10.1016/j.applthermaleng.2008.10.014

Heating Characteristics of Convection Reflow Ovens

Balázs Illés, Gábor Harsányi

Budapest University of Technology and Economics

Department of Electronics Technology

Goldmann Gy. tér 3., H-1111 Budapest, Hungary

billes@ett.bme.hu

Abstract: The inhomogeneous temperature distribution in the reflow oven can cause soldering failures. In this project, we investigate how the construction of a convection reflow oven has an affect on its heating characteristics. In the convection reflow oven itself, the heating capability is mainly dependent on the heat transfer coefficient, which in turn is mostly determined by the gas flow parameters. Therefore, we study how the construction of the reflow oven affects the flow of gas in the oven. Our conclusions are then verified with experimental results. During our experiments, temperature changes were measured at different points located around the centre of the processing area in the oven. From this data, the 3D directional characteristics of the heat transfer coefficient was calculated using the heat equation of the investigated reflow oven. We consider that our results are important for the effective thermal modelling of the reflow soldering process [1] and are also useful when calibrating and designing reflow ovens. During our work, we examine the latest reflow ovens constructed with the nozzle-matrix blower system.

Keywords: soldering, heat transfer coefficient, convection reflow oven, nozzle-matrix.

Nomenclature

Q_c	convection heat, [J]	H	nozzles – assembly distance, [m]
Q_a	absorbed heat, [J]	D	diameter of the nozzles, [m]
Q_k	parasite conduction heat, [J]	d	nozzle distance in the matrix, [m]
R_k	parasite conduction resistance, [K/W]	Re	Reynolds number of the gas
S	surface, [m^2]	Pr	Prandtl number of the gas
T_h	heating temperature, [K]	c	specific heat capacity of the measuring point, [J/kg.K]
T	temperature of the heated material, [K]	m	mass of the measuring point, [kg]
T_{DR}	temperature of the data recorder, [K]	τ	time coefficient of the heating [s]
T_{MP}	temperature of the measuring point, [K]	α	heat transfer coefficient, [$W/m^2.K$]
q_m	mass flow rate, [kg/s]	ρ	density of the gas, [kg/m^3]
v	flow rate of the gas, [m/s]	λ	thermal conductivity of the gas, [W/m.K]

1. INTRODUCTION

Reflow soldering is an important step of surface mounted technology (SMT). This process is applied when attaching surface mount devices (SMDs) to printed wiring boards (PWBs). The preparatory steps of the process are the printing of solder paste to the contact surfaces (pads) of the PWB, and the component placement onto the solder paste deposit. The reflow process then heats the entire assembly to a temperature beyond the melting point (reflow temperature) of the solder alloy. This allows the individual solder particles to melt into a single volume which can wet the soldering surfaces and form the solder joints.

Usually the heating of the assembly is achieved by a convection reflow oven containing a number of independently controllable heater zones [2]. In the latest ovens, the heater zones use the nozzle-matrix gas blower system (Fig. 1). During the soldering process, the assembled PWB is drifted on a conveyor line under these nozzle-matrices. Nowadays, most reflow ovens are designed to use double (max. 2×200 mm wide) conveyor lines, although in many cases the manufacturers use only a single conveyor line which is located in an asymmetric position in the oven.

The heating performance of convection reflow ovens mainly depends on the heat transfer coefficient (α) and can be characterized by the convection heat flow rate (Newton's law) [3– 5]:

$$\dot{Q}_c(t) = \alpha \cdot S \cdot (T_h(t) - T(t)) \qquad [\mathrm{W}] \qquad (1)$$

The factors that have an affect on α are the following: the gas used for heating, the flow rate of the gas, the gas density, the angle of incidence of the gas flow, and finally, the roughness of the heated surface [6, 7]. In our application, we consider the material of

the heater gas (nitrogen) and the roughness of the heated surface to be constants. The other parameters are characterized by the mass flow rate through an *S* surface [6, 7]:

$$q_m = \int_S \rho \cdot v \cdot dS \tag{2}$$

The inhomogeneous temperature distribution in the reflow oven can cause soldering failures. Therefore the first heating capability examinations of reflow ovens were started with simple temperature distribution measurements [8] and simulations [9, 10] (using only 2 dimensions with low resolution). But we think that nowadays, this is not enough. Several newer thermal models of the reflow process [2, 11] still do not deal with the flow parameters and the changes of α in detail, and an average value of α is being used. But our previous results (reported in [12]) have shown that the heat transfer coefficient of the entrance gas flows is highly spatial. In addition, the asymmetric conveyor line position can also cause mass transfer asymmetry in the reflow oven. This mass transfer will be greater in the direction where the gas has more opportunity to spread.

Useful simulations and numerical analysis of the forced convection [13–16] are already in existence but none can be effectively applied to the reflow soldering environment. Only a limited number of publications deal with convection reflow ovens, and unfortunately these contain mistakes. Eveloy [17, 18] and Powel [19] built CFD models for special convection reflow ovens, but these totally differed in construction to the reflow ovens applied in mass production. In addition, Eveloy studied the temperature interval between 50 and 80°C, which is a too low temperature in the case of reflow soldering. Belov [20] pursued a similar path and only examined the preheating phase of the reflow soldering between the range of 100 – 120°C.

A method for optimizing the heating capability of convection reflow ovens has been published [21], but this deals only with the geometry and dimensions of the nozzles and

not the characterization and the measurement of the α parameter. An approximation of the α parameter in convection reflow ovens (with nozzle-matrix blower system) already exists [22]:

$$\alpha = \frac{\lambda}{2 \cdot d} \cdot G\left(g, \frac{H}{d}\right) . \mathrm{Re}^{\frac{2}{3}} \cdot \left[1 + \left(\frac{H/d}{0.6/\sqrt{g}}\right)^6\right]^{-0.05} \cdot \mathrm{Pr}^{0.42} \tag{3.1}$$

$$G = 2\sqrt{g}\,\frac{1 - 2.2\sqrt{g}}{1 + 0.2(H/D - 6)\sqrt{g}} \tag{3.2}$$

$$g = \frac{\pi}{4}\left(\frac{D}{r}\right)^2 \tag{3.3}$$

The expression (3) shown above, has been derived from systematic series of experiments. But unfortunately this method only gives an average value of α and does not deal with the changes of the flow parameters in the oven and its affects on the α parameter.

Consequently, it is important to examine how the construction of the reflow oven has an affect on its spatial heating performance. This gives valuable information about the properties of the oven and is important in the simulations of reflow soldering process [1].

2. EXPERIMENTAL

In our project, we examined a convection reflow oven which was constructed with a nozzle-matrix blower system and 8 separated zones (7 out of 8 being heater zones). The oven had a single conveyor line located in an asymmetric position in the oven. We modelled the gas flow in the oven on the following criteria which was that the vertical gas streams from the nozzle-matrix join into a continuous radial flow layer above the board [23, 24].

At a given point on the board the flow direction of the radial layer is determined by a so called “balance line” (defined in the remaining paragraphs of this section). The schematic view of the gas flows can be seen along the moving direction (x axis) in Fig 2(a) and perpendicular to it (y axis) in Fig 2(b). The zero point of the coordinate system was placed into the geometrical centre of the test board. The direction of a gas stream from a given nozzle depends on the position of the board in the oven. The balance line marks that location where the main flow direction is changed. Along the x axis, this has an oscillation near the centre of the test board caused by the movement of the board. However, the system is symmetrical along the moving direction (x axis) of the board. This enables us to assume that the transported mass and energy are nearly equal in the $-x$ and $+x$ directions during the soldering.

As we have already mentioned, the conveyor line is located in an asymmetric position in the oven ($h_1 \neq h_2$). The board does not move along the y axis during the process, therefore the balance line of the y axis is fixed but in an asymmetric position. It moves from the centre into the $-y$ direction (Fig. 2(b)). From this, our assumption was that when the asymmetric position of the conveyor occurs, the transported mass and energy should be larger in the $+y$ direction than in the $-y$ direction.

The transported energy in the radial flow layer also depends on the distance from the board (z direction), and not only the x and y directions, due to the method of gas blowing [23, 24]. Therefore our aim was to investigate the α parameter of the radial flow layer depending on its location These effects could be investigated by the determination of the 3D direction characteristics of the heat transfer coefficient.

2.1 The Measuring System

As we have already discussed in the Introduction, we needed to determine the pressure, the density and the flow rate of the gas for the calculation of α. The exact measurement of these parameters would be very complicated because of the extreme conditions in the reflow oven (small space, high temperature etc). Our alternative solution was to examine the heating characteristics of the oven. We measured the temperature changes at different locations in the radial flow layer. The α parameters were then calculated using the heat equation of the investigated reflow oven:

$$Q_a = Q_c + Q_k \tag{8}$$

Convection reflow ovens do not contain infra-radiation tubes and the inside of the ovens are made from polished stainless steel which means that their emissivity is very low (~0.1), therefore we can neglect the radiation heat [16–18].

The temperature changes should be measured with the minimum of disturbance to the gas flow. Therefore, we would have to use point probes for this purpose. We chose K-Type rigid (steel coat) thermocouples with a 1mm diameter. Their rigid coating ensured that the thermocouples kept in the correct position while travelling through the reflow oven.

The common height of the applied SMDs by electronics industry is between 1–15mm. We divided this range to 6 parts: 1, 3, 6, 9, 12 and 15mm where the measurements were taken. The probes were fixed in a measuring gate (measuring box) which held them in position (Fig. 3). The front and the rear end of the gate were opened so the radial flow could pass through it, but the roof of the gate protected the probes from the disturbing effect of the entering gas streams. The gate was made from FR4 (d

= 0.8mm), with a width and length of 30mm and a height of 20mm. The probes were put into the gate through small holes on the left lateral side.

An advantage of this arrangement was that the probes only obstruct the flow at the measuring points because they were parallel to the radial flow layer. The obstruction and measuring points were overlapped and the disturbance of the radial layer was minimal.

We used an empty FR4 test board, 175x175mm in area. Twelve Measuring Locations (MLs) were chosen, each equally located around a circle whose centre aligned with the centre of the test board. The circle had a radius of 30mm (Fig. 4). The measuring gate was positioned on the MLs facing towards the centre of the test board.

2.2 Data processing and calculation

For the measurements we used the "Datapacq" type system set to a sampling time of 0.1 s. The data was processed using both the "Reflow Tracker" and "Matlab 7.0" programs. As we expected, the measured curves (the temperature changes) showed exponential saturation.

We had to fit analytical curves to the measured curves for the calculations of α. As we have already mentioned, the measured curves can be modelled with exponential saturation:

$$T(t) = (T_h - T(t_0)) \cdot (1 - e^{-t/\tau}) \tag{9}$$

where the time coefficient of the heating is:

$$\tau = t_r / \ln\left(1 - (T(t_r) - T(t_0))/(T_h - T(t_0))\right) \tag{10}$$

Although we knew the set temperatures in each heater zone, these were not equal to T_h as the measuring device (just like the assemblies) had a cooling effect on the heater

zone itself. This effect very much depended on the time and the location of the measuring device in the oven, because the oven itself tried to maintain a set temperature. Therefore, the exact T_h values of the measured curves had to be calculated by using an iteration curve fitting. The T_h was iterated from the value of $T(t_r)$ using 0.01°C increments in temperature. At each iteration step, the model curve was fitted onto the measured curve. The iteration stopped when the fitting failure reached the minimal value.

In Fig. 5, the dashed line curve is calculated with only one T_h value (one fitting curve) for the whole curve. But in reality, the T_h is changing during the measurement. If we then apply two T_h values (two fitting curves) – one for the first part $[t_0, t_1]$ and one for the second part $[t_1, t_r]$ of the curve – the matching is much better (continuous line). Based on our observations about T_h, the model curve (Eq. (9)) has been modified:

$$T(t) = (T_h(t) - T(t_0)) \cdot (1 - e^{-t/\tau(t)}) \tag{11}$$

where $T_h(t) = \begin{bmatrix} T_{h1}|_{0-t_1} \\ T_{h2}|_{t_1-t_r} \end{bmatrix}$, and two time coefficients $\tau(t) = \begin{bmatrix} \tau_1|_{0-t_1} \\ \tau_2|_{t_1-t_r} \end{bmatrix}$ are needed. The convection heat is calculated by the integration of Eq. (1) to the time interval of the heating $[t_0, t_r]$:

$$\begin{aligned} Q_c &= \int_{t_0}^{t_r} \dot{Q}_c(t)\, dt = \int_{t_0}^{t_r} \alpha \cdot S \cdot (T_h(t) - T(t)) = \\ &= \alpha \cdot S \cdot \left[(T_{h1} - T(t_0)) \cdot \tau_1 \cdot \left(1 - e^{-t_1/\tau_1}\right) + (T_{h2} - T(t_1)) \cdot \tau_2 \cdot \left(1 - e^{-tr/\tau_2}\right) \right] \end{aligned} \tag{12}$$

The amount of absorbed heat is calculated as:

$$Q_a = c \cdot m \cdot (T(t_r) - T(t_0)) \tag{13}$$

The thermocouples (except the measuring point) are insulated from the steel coat with a glass wool layer which has a very bad thermal conductivity (~1 W/m.K) to

decrease the impact of the environment. However, we had to consider the parasite conduction resistances (R_k) between the Data Recorder (DR) and the Measuring Points (MPs). Our results proved that the parasite conduction effect should be considered in case of thermocouple measurements although on some occasions it was ignored [25, 26].

The MP was modelled as a sphere, as shown in Fig. 6. We ignored the conduction behavior of the MP because of its small dimensions. The thermal potential difference between the DR and the MP $\left(T_{DR} - T_{MP}\right)$ generated a parasite conduction heat flux $\dot{Q}_k$ on the conduction resistance R_k. Unfortunately, the exact values of R^* and T_{DR} remain unknown and $\dot{Q}_k$ is not calculable. Therefore we used an offset calibration of the system to eliminate the impact of $\dot{Q}_k$.

Two different arrangements of the measuring system should be used (Fig. 6). In the first case, the DR is positioned after the MP. This results in $T_{MP} > T_{DR}$ and Q_k having a negative value in the heat equation (8). In the second (reverse) case, Q_k has positive value in (8). Therefore, the addition of the heat equations in the two different cases eliminates the effect of $\dot{Q}_k$.

In order to avoid this long-drawn method for all measuring points, we had to define a correction number. We compared 2×20 measurement results of the different arrangements and concluded that the α values of the first arrangement were about 9–11% larger than the α values of the second arrangement. As a consequence, we could eliminate the effect of $\dot{Q}_k$ if we defined $k = 0.95$ as a correction number and applied it to the results of the first arrangement. The α values were calculated according to the expressions (8), (12) and (13):

$$\alpha = \frac{k \cdot Q_a}{S \cdot \int_{t_0}^{t_r} (T_h(t) - T(t))} \qquad [\mathrm{W/m^2K}] \qquad (14)$$

The absolute inaccuracy of the thermocouples was ±0.5 °C, but it did not cause measurement failure, due to the integration of the temperature in Eq. (14).

The materials of the thermocouples are NiCr (90:10) – NiAl (95:5). The physical properties of these materials are well known, so the necessary parameters of the MPs for the calculations can be exactly determined (Tab. 1).

3. Results and Discussion

We used a soak thermal profile for leaded solders during the measurements. The set temperatures of the heater zones are shown in Tab. 2. We could not process the results of the 7th (2nd peak zone) zone because the temperature change in this zone was too small, only 1–2°C.

The α parameters of the measuring location ML_0, ML_{90}, ML_{180} and ML_{270} can be seen in Fig. 7. We observed minor efficiency differences between the heater zones. The maximum deviation in the results was ±5 W/m^{2}K. This effect was probably caused by the inhomogeneity of the gas circulation system and/or the different contamination level of the nozzle-matrices.

We observed that there were major heating capability differences between the MLs caused by the construction of the oven. The α parameters were much larger (80–120%) in the MLs where the measuring gate stood parallel or near parallel to the walls of the oven, than those where it stood perpendicular or near perpendicular to the walls. In addition, there were also considerable heating capability differences (30–40%) between

the MLs where the measuring gate faced the opposite walls (ML_{90} and ML_{270}). This was caused by the asymmetrical position of the conveyor line in the oven (Fig. 2(b)). We examined only minor deviations (1–5%) between the MLs where the measuring gate faced the zone ends (ML_0 and ML_{180}).

In addition, the value of α depends on the measuring height. It increases when getting closer to the test board until a given distance (peak value is near 3-4mm from the board). This effect is caused by the growth of density and flow rate in the radial layer towards the test board, as proved in our previous work with the CFD model of the entering gas streams [27]. However, the friction becomes considerably higher at the closest ambience of the board (0-1 mm). This slows the flow rate [27–29] more than the growth of the density, and this effect decreases α.

The α values of ML_0 to ML_{330} can be presented separately in each heater zone as 3D directional characteristics of the heat transfer coefficient. This means that we illustrate the α values above the *x*-*y* plane according to the MLs and the measuring height around the centre of the board. The appropriate values are attached because of the better visualization: the values of a given measuring height are attached with a horizontal curve and the values of a given ML are attached with a vertical curve. In this form, our results are more expressive because the heating capability is analyzable in each direction. Fig. 8 shows the 3D directional characteristics of α in the 6^{th} heater zone. In the main axes (*x* and *y*), the minimum and maximum values of α are marked in Fig. 8.

4. CONCLUSIONS

The measured α values (Fig. 7) prove that the construction of the reflow oven (the position of the conveyor line) considerably affects the heating characteristics of the oven. The mass transfer (and α) will be higher in the direction where the gas has more opportunity to spread. We also have observed that there are major heating capability differences between each of the MLs. The α parameters are much larger (80–120%) in the MLs where the measuring gate stands parallel (or near parallel) to the walls of the oven, than those where the measuring gate stands perpendicular (or near perpendicular) to the walls (Fig. 7). There are also considerable heating capability differences (30–40%) between MLs where the measuring gate faces the opposite walls (ML_{90} and ML_{270}). This is caused by the asymmetrical position of the conveyor line in the oven (Fig. 2(b)).

In addition, the value of α depends on the measuring height. It increases when getting closer to the test board until a given distance (peak value is near 3-4mm from the board). This is caused by the growth of the density and flow rate in the radial flow layer towards the test board, as we have demonstrated in our previous work with the CFD model of the entering gas streams [27]. However, the friction becomes considerably higher at the closest ambience of the board (0-1 mm) and it slows the flow rate [27–29] more than the density growth which decreases α.

The asymmetrical directional characteristics of α (Fig. 8) show that the transported convection heat is spatial which can cause soldering failures. But, armed with the 3D direction characteristics of α, effective thermal simulations and failure predictions as well as heating and layout optimizations can be effectively undertaken.

REFERENCES

[1] B. Illés, G. Harsányi, 3D Thermal Model to Investigate Component Displacement Phenomenon during Reflow Soldering, Microelectronics Reliability 48 (2008) 1062– 1068.

[2] D.C. Whalley, A simplified reflow soldering process model, Journal of Materials Processing Technology 150 (2004) 134–144.

[3] A. Castell, C. Solé, M. Medrano, J. Roca, L. F. Cabeza, D. García, Natural convection heat transfer coefficients in phase change material (PCM) modules with external vertical fins, Applied Thermal Engineering 28 (2008) 1676–1686.

[4] Y. Gao, S. Tse, H. Mak, An active coolant cooling system for applications in surface grinding, Applied Thermal Engineering 23 (2003) 523–537.

[5] X. Zhao a, J.M. Li, S.B. Riffat, Numerical study of a novel counter-flow heat and mass exchanger for dew point evaporative cooling, Applied Thermal Engineering 28 (2008) 1942–1951.

[6] F. Incropera, Fundamentals of Heat and Mass Transfer, 2001, 5th Ed., Wiley.

[7] W. Kays, M. Crawford, B. Weigand, Convective Heat and Mass Transfer, 2004, 4th Ed., McGraw-Hill Professional.

[8] B. Rosu, P. Reyes-Turcu, D. Simion-Zanescu, Thermal management system for reflow oven, IEEE Proceedings of 28th Int. Spring Seminar on Elctronics Technology, Wr. Neustadt, Austria, 2006, pp.294–298.

[9] F. Sarvar, P.P. Conway, Effective modelling of the reflow soldering process: basis construction and operation of a process model, IEEE Trans. Components Packaging Manuf. Technol. Part C: Manuf. 21 (2) (1998) 126–133.

[10] C-H. Wu, K. Srihari, A.J. McLenaghan, A knowledge-based thermal profile identification advisor for surface mount PCB assembly, Int. Journal of Advanced Manufacturing Technology 11 (1996) 343–352.

[11] N.V. Steenberge, P. Limaye, G. Willems, B. Vandevelde, I. Schildermans, Analytical and finite element models of the thermal behavior for lead-free soldering processes in electronic assembly, Microelctronics Reliability 47 (2007) 215-222.

[12] B. Illés, O. Krammer, G. Harsányi, Zs. Illyefalvi-Vitéz, 3D Investigations of the Internal Convection Coefficient and Homogeneity in Reflow Ovens, IEEE Proceedings of 30th Int. Spring Seminar on Elctronics Technology, Cluj-Napoca, Romania, 2007, pp.320-325.

[13] G. Juncu, A numerical study of momentum and forced convection heat transfer around two tandem circular cylinders at low Reynolds numbers. Part II: Forced convection heat transfer, Inernational Journal of Heat and Mass Transfer 50 (2007) 3799-3808.

[14] J. Yin, B.C. Wang, J.D. Bergstrom, Large-eddy simulation of combined forced and natural convection in a vertical plane channel, Inernational Journal of Heat and Mass Transfer 50 (2007) 3848-3861.

[15] F. Erdogdu, A review on simultaneous determination of thermal diffusivity and heat transfer coefficient, Journal of Food Engineering 86 (2008) 453–459.

[16] P. Verboven, N. Scheerlinck, J. De Baerdemaeker, B. M. Nicolai, Computational fluid dynamics modelling and validation of the temperature distribution in a forced convection oven, Journal of Food Engineering 43 (2000) 61– 73.

[17] V. Eveloy, P. Rodgers, M.S.J. Hashmic: Application of numerical analysis to the optimisation of electronic component reliability screening and assembly processes, Journal of Materials Processing Technology 155–156 (2004) 1788 – 1796.

[18] V. Eveloy, P. Rodgers, Prediction of Electronic Component-Board Transient Conjugate Heat Transfer, IEEE Transactions on Components and Packaging Technologies 28 (2005) 817–829.
[19] R.E. Powell, Development of Convective Solder Reflow and Projection Moiré System and FEA Model for PWBA Warpage Prediction, Ph.D. thesis work, 2006.
[20] I. Belov, M. Lindgren, P. Leisner, F. Bergner, R. Bornoff, CFD Aided Reflow Oven Profiling for PCB Preheating in a Soldering Process, IEEE Proceedings of EuroSime Conference, London, England, 2007, pp. 1–8.
[21] M. Yamane, N. Orita, K. Miyazaki, W. Zhou, Development of New Model Reflow Oven for Lead-Free Soldering, Furukawa Review 26 (2004) 31–36.
[22] M. Inoue, T. Koyanagawa, Thermal Simulation for Predicting Substrate Temperature during Reflow Soldering Process, IEEE Proceedings of 55th Electronic Components and Technology Conference, Lake Buena Vista, Florida, 2005, pp.1021-1026.
[23] B. Illés, O. Krammer, G. Harsányi, Zs. Illyefalvi-Vitéz, Modelling Heat Transfer Efficiency in Forced Convection Reflow Ovens, IEEE Proceedings of 29th Int. Spring Seminar on Elctronics Technology, St. Marienthal, Germany, 2006, pp.80-85.
[24] B. Illés, O. Krammer, Variation of Gas Flow Parameters in Forced Convection Reflow Oven, Proceedings of 13th SIITME Conference, Bia-Mare, Romania, 2007, pp.27-31.
[25] G.H. Su, Y.W. Wu, K. Sugiyama, Natural convection heat transfer of water in a horizontal gap with downward-facing circular heated surface, Applied Thermal Engineering 28 (2008) 1405–1416.
[26] Y. Islamoglu, C. Parmaksizoglu, The effect of channel height on the enhanced heat transfer characteristics in a corrugated heat exchanger channel, Applied Thermal Engineering 23(2003) 979–987.
[27] B. Illés, Direction Characteristics of the Heat Transfer Coefficient in Convection Reflow Oven – Part I: Parameters and Gas Flow Model, Proceedings of 14th SIITME, Brasov, Romania, 2008, pp. 60 – 64.
[28] J.R. Wang, J.C. Min, Y.Z. Song, Forced convective cooling of a high-power solid-state laser slab, Applied Thermal Engineering 26 (2006) 549–558.
[29] Y.P. Cheng, T.S. Lee, H.T. Low, Numerical simulation of conjugate heat transfer in electronic cooling and analysis based on field synergy principle, Applied Thermal Engineering 28 (2008) 1826–1833.

List of Figures:

Fig. 1. Nozzle-matrix of a heater zone.

Fig. 2(a). Gas flows above the board (cross-sectional view, *x* axis).

Fig. 2(b). Gas flows above the board (cross-sectional view, y axis).

Fig. 3. The measuring system.

Fig. 4. Measuring locations (MLs) on the test board (upper view).

Fig. 5. Analytical curve fitting.

Fig. 6. Offset calibration of the measuring system.

Fig. 7. Results of ML_0, ML_{90}, ML_{180} and ML_{270}.

Fig. 8. 3D directional characteristics of α in the 6^{th} heater zone.

List of Tables:

Tab. 1. Parameters of the measuring points (MPs).

Tab. 2. Set temperatures in the heater zones.

Tab. 1.
Parameters of the measuring points (MPs).

Density, ρ [kg/m^3]	8210
Specific heat capacity, c [J/kg.K]	474
Diameter of the MPs, r_{MP} [m]	4×10^{-4}
Effective surface of the MPs, $A = 4/3 \cdot \pi \cdot r_{MP}^{\ 2}$ [m^2]	1.04×10^{-6}
Volume of the MPs, $V = 4/6 \cdot \pi \cdot r_{MP}^{\ 3}$ [m^3]	1.31×10^{-10}
Mass of the MPs, $m = \rho \cdot V$ [kg]	1.07×10^{-6}

Tab. 2.
Set temperatures in the heater zones.

Heater zone	Temperature [°C]
1	120
2	150
3	150
4	160
5	180
6 (peak 1)	245
7 (peak 2)	235

Fig. 1. Nozzle-matrix of a heater zone.

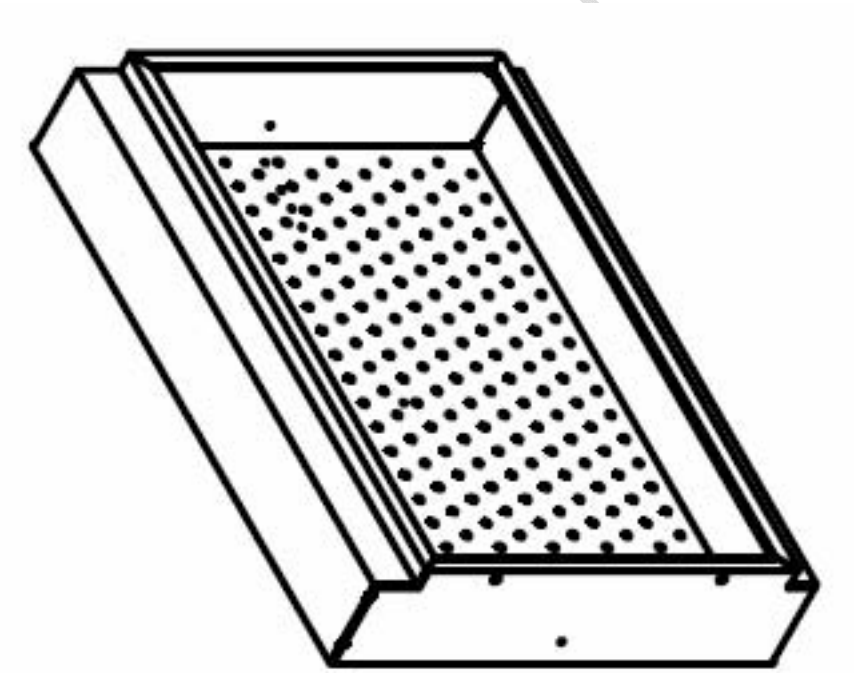

Fig. 2(a). Gas flows above the board (x axis)

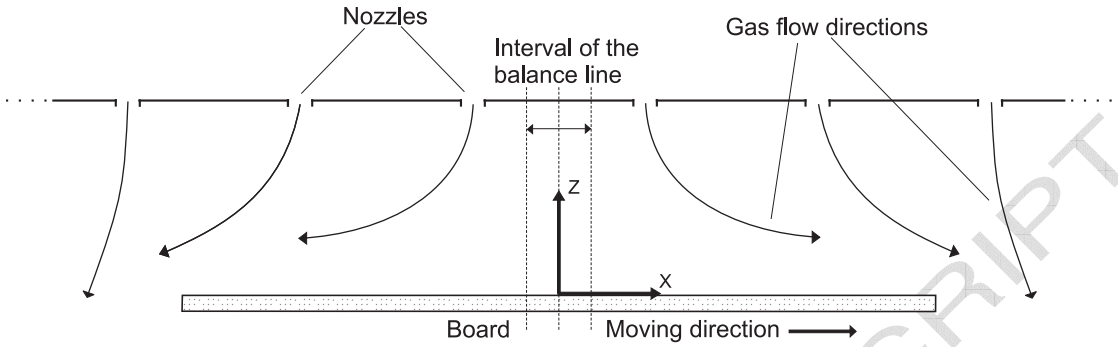

Fig. 2(b). Gas flows above the board (y axis)

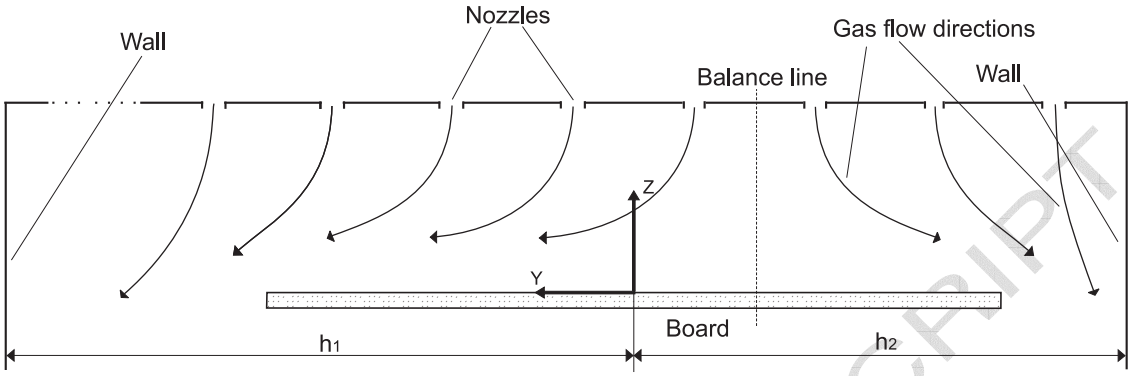

Fig. 3. The measuring system.

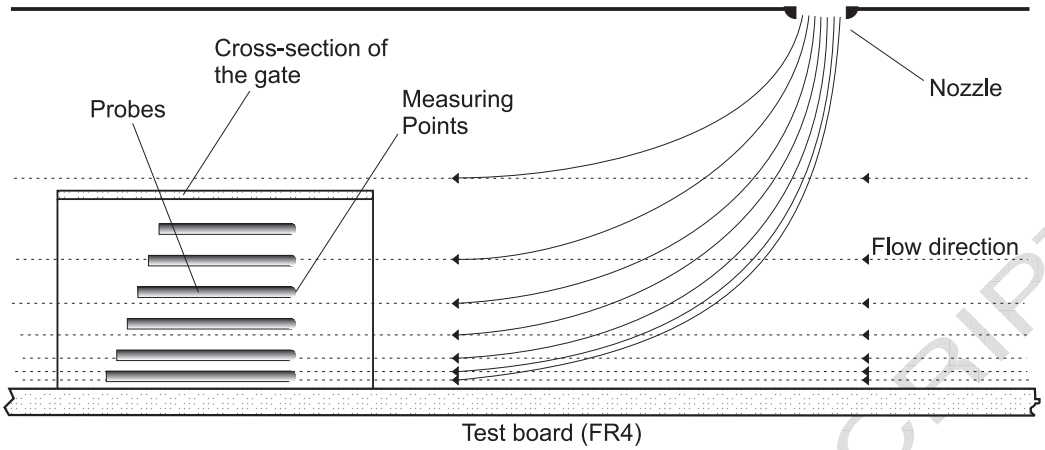

Fig. 4. Measuring locations (MLs) on the test board (upper view)

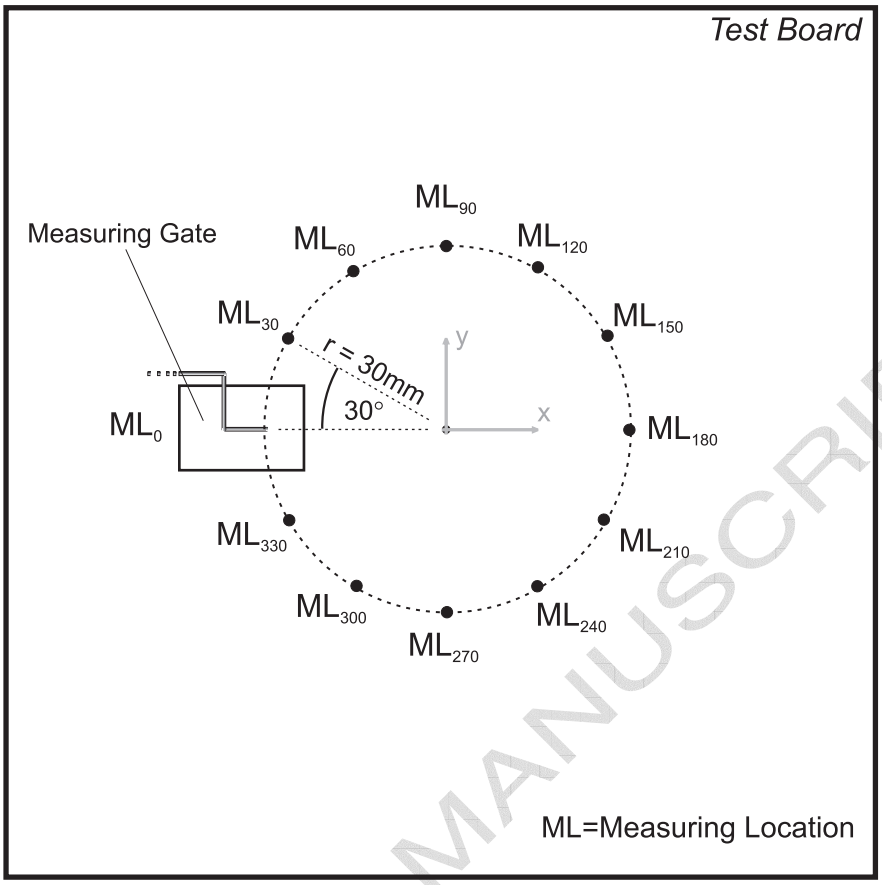

Fig. 5. Analytical curve fitting.

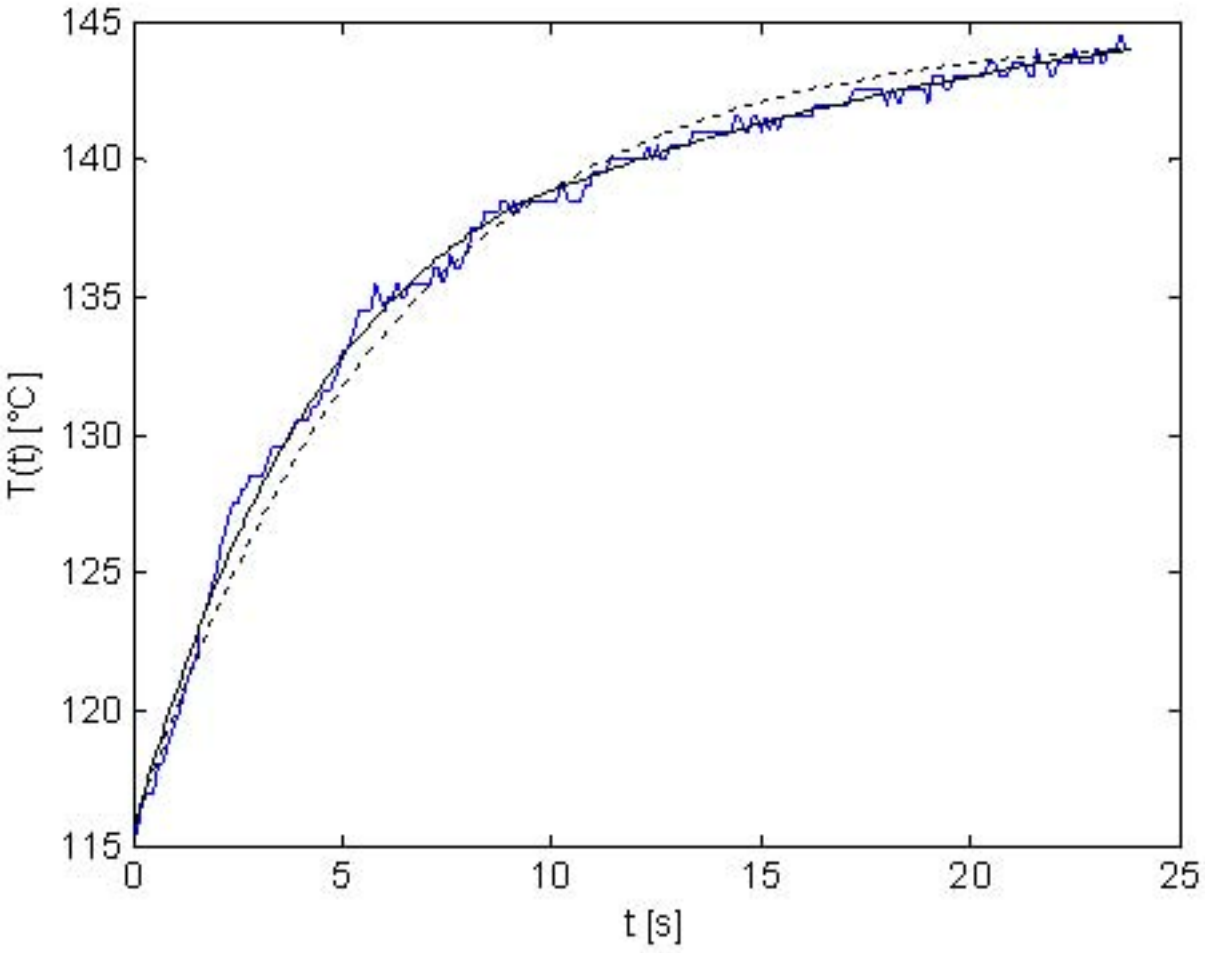

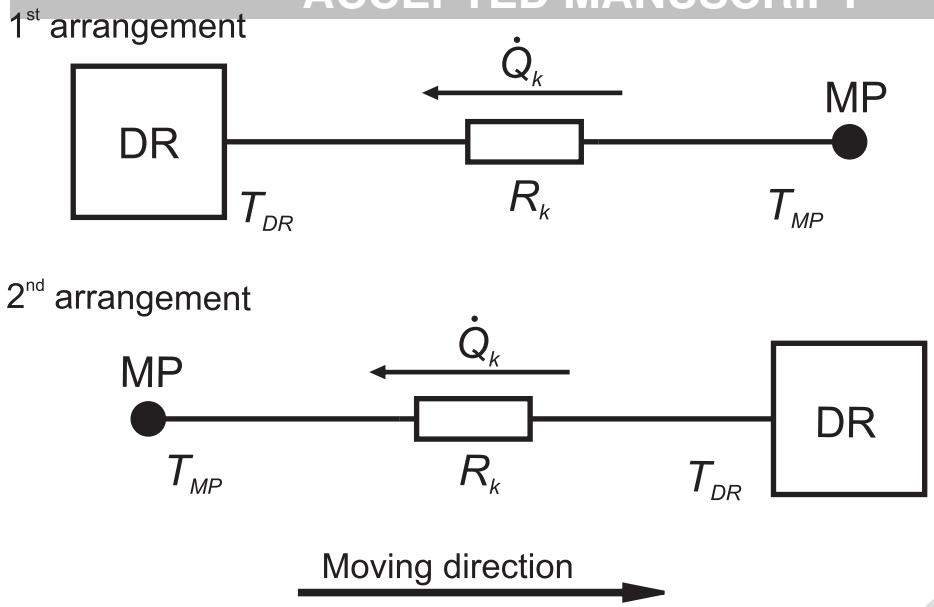

Fig. 6. Offset calibration of the measuring system.

Fig. 7. Results of ML0, ML90, ML180 and ML270.

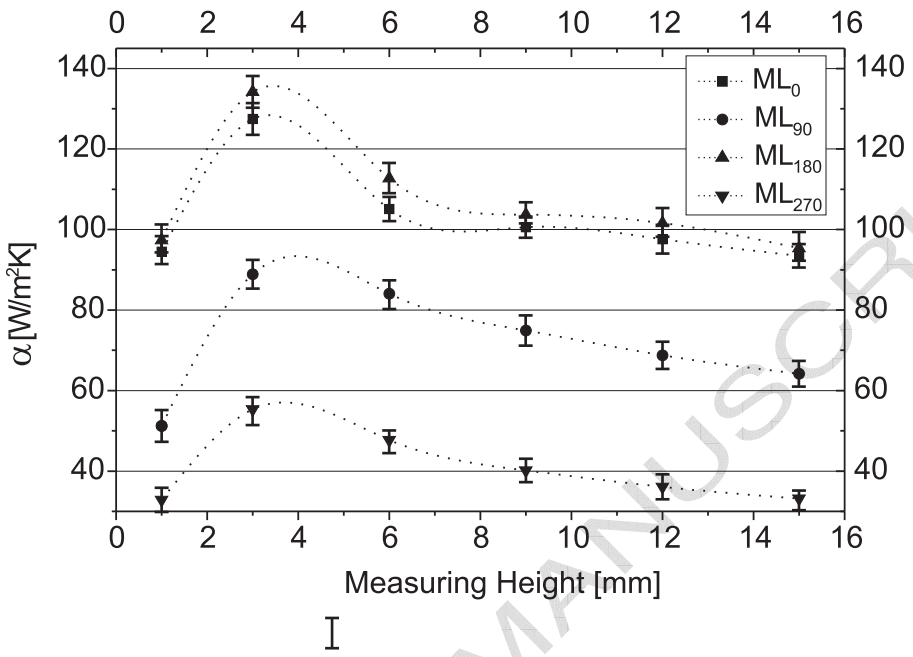

Fig. 8. 3D dir. characteristics of alpha in the 6th zone.